CrossMark

Mass Measurements for Two Binary Pulsars Discovered in the PALFA Survey

W. W. Zhu[1,2] , P. C. C. Freire[1] , B. Knispel[3,4], B. Allen[3,4,5] , B. W. Stappers[6], A. G. Lyne[6], S. Chatterjee[7] , J. M. Cordes[7] ,
F. Crawford[8] , J. S. Deneva[9,18] , R. D. Ferdman[10] , J. W. T. Hessels[11,12] , V. M. Kaspi[13], P. Lazarus[1], R. Lynch[14,15] ,
S. M. Ransom[15] , K. Stovall[16] , and J. Y. Donner[1,17]

[1] Max-Planck-Institut für Radioastronomie, Auf dem Hügel 69, D-53131 Bonn, Germany; pfreire@mpifr-bonn.mpg.de
[2] CAS Key Laboratory of FAST, NAOC, Chinese Academy of Sciences, Beijing 100101, People's Republic of China
[3] Max-Planck-Institut für Gravitationsphysik, D-30167 Hannover, Germany
[4] Leibniz Universität Hannover, D-30167 Hannover, Germany
[5] Physics Department, University of Wisconsin–Milwaukee, Milwaukee WI 53211, USA
[6] Jodrell Bank Centre for Astrophysics, School of Physics and Astrophysics, University of Manchester, Manch., M13 9PL, UK
[7] Cornell Center for Astrophysics and Planetary Science and Department of Astronomy, Cornell University, Ithaca, NY 14853, USA
[8] Department of Physics and Astronomy, Franklin and Marshall College, Lancaster, PA 17604-3003, USA
[9] George Mason University, 4402 University Drive, Fairfax, VA 22030, USA
[10] Faculty of Science, University of East Anglia, Norwich Research Park, Norwich NR4 7TJ, UK
[11] ASTRON, the Netherlands Institute for Radio Astronomy, Postbus 2, 7990 AA, Dwingeloo, The Netherlands
[12] Anton Pannekoek Institute for Astronomy, University of Amsterdam, Science Park 904, 1098, XH Amsterdam, The Netherlands
[13] Department of Physics, McGill University, Montreal, QC H3A 2T8, Canada
[14] Green Bank Observatory, PO Box 2, Green Bank, WV, 24944, USA
[15] NRAO, Charlottesville, VA 22903, USA
[16] National Radio Astronomy Observatory, 1003 Lopezville Road, Socorro, NM, 87801, USA
[17] Fakultät für Physik, Universität Bielefeld, Postfach 100131, D-33501 Bielefeld, Germany

Abstract

In this paper, we present the results of timing observations of PSRs J1949+3106 and J1950+2414, two binary millisecond pulsars (MSPs) discovered in data from the Arecibo ALFA pulsar survey (PALFA). The timing parameters include precise measurements of the proper motions of both pulsars, which show that PSR J1949 +3106 has a transversal motion very similar to that of an object in the local standard of rest. The timing also includes measurements of the Shapiro delay and the rate of advance of periastron for both systems. Assuming general relativity, these allow estimates of the masses of the components of the two systems; for PSR J1949+3106, the pulsar mass is $M_p = 1.34_{-0.15}^{+0.17} M_\odot$ and the companion mass $M_c = 0.81_{-0.05}^{+0.06} M_\odot$; for PSR J1950+2414 $M_p = 1.496 \pm 0.023 M_\odot$ and $M_c = 0.280_{-0.004}^{+0.005} M_\odot$ (all values have 68.3% confidence limits). We use these masses and proper motions to investigate the evolutionary history of both systems: PSR J1949+3106 is likely the product of a low-kick supernova; PSR J1950+2414 is a member of a new class of eccentric MSP binaries with an unknown formation mechanism. We discuss the proposed hypotheses for the formations of these systems in light of our new mass measurements.

Key words: binaries: general – pulsars: general – pulsars: individual (PSR J1949+3106, PSR J1950+2414) – stars: neutron

1. Introduction

1.1. The PALFA Pulsar Survey

The PALFA survey (Cordes et al. 2006; Lazarus et al. 2015), currently being carried out with the Arecibo Observatory, has thus far discovered 189 pulsars.[19] The high spectral and time resolution of the data are optimized for the discovery of millisecond pulsars (MSPs; defined here as recycled pulsars with a spin period $P < 25$ ms) at high values of dispersion measure (DM), enabling searches for MSPs to great distances into the Galactic plane. This approach is now well demonstrated, with the discovery of 30 new MSPs, most with large DMs compared to the previous population and large distances (Champion et al. 2008; Knispel et al. 2010, 2011, 2015; Crawford et al. 2012; Deneva et al. 2012; Allen et al. 2013; Scholz et al. 2015; Stovall et al. 2016). The PALFA survey uses the PRESTO software package (Ransom 2011) for pulsar searches.

The instantaneous sensitivity of the Arecibo 305 m telescope means that the survey can achieve considerable depth with relatively short pointings (about 4.5 minutes); this makes it sensitive to highly accelerated systems. It is partly for this reason that the survey has already discovered three new relativistic pulsar–neutron star (PSR–NS) systems: PSRs J1906 +0746 (Lorimer et al. 2006), a system where the pulsar we detect is the second-formed NS, J1913+1102 (Lazarus et al. 2016), a system with a likely mass asymmetry and J1946 +2052 (Stovall et al. 2018), the most compact PSR–NS system known. This survey has also discovered the first repeating fast radio burst (Spitler et al. 2014, 2016).

1.2. The Pulsars

PSR J1949+3106 is one of the two new MSPs announced by Deneva et al. (2012). It has a spin period of 13.1 ms, and it is in a binary system with an orbital period of 1.95 days. The projected semimajor axis of its orbit ($x = 7.29$ lt-s) implies that it has a massive companion; the small orbital eccentricity ($e = 0.000043$) implies that this massive companion is a white dwarf (WD) star. In the discovery paper, Deneva et al. (2012)

also measured the Shapiro delay in this system and determined the masses of the pulsar and its companion: $m_p = 1.47^{+0.43}_{-0.31} M_\odot$ and $m_c = 0.85^{+0.14}_{-0.11} M_\odot$. Although the Shapiro delay had been detected with high significance, the uncertainties of the published masses are too large to be astrophysically useful.

PSR J1950+2414 was found by the Einstein@Home pipe-line (Allen et al. 2013); its discovery and early timing results were described by Knispel et al. (2015). It is a 4.3 ms pulsar in a 22.2 day orbit with a companion that is likely to be a low-mass WD. The unusual characteristic of this system is its orbital eccentricity, $e = 0.0798$, which is much larger than those of most MSP–WD systems. This system is not unique in this respect; there are four other similar systems with orbital periods between 22 and 32 days and eccentricities of the order of 0.1 (PSR J2234+0611, Deneva et al. 2013; Stovall et al. 2019; PSR J1946+3417, Barr et al. 2013, 2017; PSR J0955 −6150, Camilo et al. 2015; PSR J1618−3921, Octau et al. 2018). Such similarities are not expected from a chaotic process like the triple disruption that is thought to have formed the unusual eccentric MSP—main-sequence star PSR J1903+0327 (Champion et al. 2008; Freire et al. 2011); however, as we show later, the exact formation mechanism for these binaries is still unknown.

For PSR J1950+2414, Knispel et al. (2015) measured the rate of advance of periastron, $\dot\omega = 0\overset{\circ}{.}0020(3)$ yr^{-1}. Assuming this is solely an effect of general relativity (GR), they estimated that the implied total mass of the system, M, is 2.3(4) $M_\odot$. No other PK parameters were measured, so it was not possible to separate the component masses. Although the measurement of $\dot\omega$ is highly significant, the uncertainty on the resulting M was too large to draw any interesting conclusions about the system.

1.3. Motivation and Structure of the Work

In this work, we present the results of continued timing of these two binary systems. The main aim of this project was to measure the proper motions of the two systems more precisely and to improve (as in the case of PSR J1949+3106) or to obtain (as in the case of PSR J1950+2414) masses for the MSPs and their companions.

Measuring NS masses is important for several reasons. First, their measurement allows, in some cases, precise tests of the nature of gravitational waves (Freire et al. 2012) and of the strong equivalence principle (Archibald et al. 2018), which represent stringent tests of GR and alternative theories of gravity. Large NS masses, as in the case of PSR J0348+0432 (Antoniadis et al. 2013) and PSR J0740+6620 (Thankful Cromartie et al. 2019) introduce stringent constraints on the equation of state for superdense matter, a fundamental problem in nuclear physics and astrophysics (see, e.g., Özel & Freire 2016 and references therein). Apart from this, measuring more NS masses is important for understanding the relation between the masses of the NS components and the orbital and kinematic properties of the systems, which are a product of supernova physics (see, e.g., Tauris et al. 2017 and references therein). Measuring the masses of NSs in PSR–NS and PSR–massive WD systems, where there was little accretion, is important for establishing the distribution of NS birth masses (see, e.g., Cognard et al. 2017 and references therein). Finally, measuring MSP masses is important for understanding the role that strong recycling (with potentially significant amounts of matter being accreted) have on the observed mass distribution. In this respect, it is important to determine whether the observed MSP

mass distribution is unimodal or bimodal (Antoniadis et al. 2016b).

Many of these applications require an improvement in the statistics of well-measured NS masses, and some specifically require an increase in the number of precise MSP mass measurements. Our initial analysis of the two pulsars studied in this paper found that, with adequate timing data, they would yield good mass measurements; this initial expectation was, as we show below, largely confirmed.

In Section 2, we will present the new observations we have made for this project and describe briefly how the resulting data was reduced. In Section 3, we present the timing results, with a particular focus on the proper motion and the mass measure-ments. Finally, in Section 4, we discuss the implications of these measurements for the origin and evolution of these systems.

2. Observations and Data Reduction

2.1. Observations

For both systems, we reuse the topocentric pulse times of arrival (ToAs) used in their published timing; for detailed descriptions see Deneva et al. (2012) for PSR J1949+3106 and Knispel et al. (2015) for PSR J1950+2414. For PSR J1949 +3106, the data set is dominated by Arecibo data taken with the Wideband Arecibo Pulsar Processors (WAPPs; Dowd et al. 2000). For PSR J1950+2414, the setup was similar to that used during the PALFA survey (which uses the Mock spectrometers as a backend), but on dedicated timing campaigns the Puerto Rico Ultimate Pulsar Processing Instrument (PUPPI) was used, mostly with the "L-wide" receiver, which is sensitive to radio frequencies between 1170 and 1730 MHz. We present here the two pulsar's pulse and polarization profile (Figure 1) in the 1170–1730 MHz band.

Most of the new data on both systems were taken with PUPPI in coherent dedisperison mode and the L-wide, in the way described by Knispel et al. (2015). All PUPPI data for both pulsars were processed as independent 100 MHz blocks; the ToAs are derived from the integrated pulse profiles within each 100 MHz block using the standard PSRCHIVE[20] (Hotan et al. 2004) routines as described in the aforementioned works. For PSR J1949+3106, we used separate profile templates for each 100 MHz subband to derive ToAs that account for any frequency-dependent evolution of the profile shape (This method was earlier used by Donner et al. 2019, where further details can be found.) This has significantly improved the timing precision of this pulsar relative to the standard single-template method, part of the reason is the strong profile evolution for this pulsar as a function of frequency (Deneva et al. 2012). For PSR J1950+2414, this method did not improve the timing noticeably, so we used TOAs derived from the standard single-template method.

For PSR J1949+3106, more than half of the additional PUPPI data resulted from the North American Nanohertz Observatory for Gravitational Waves (NANOGrav) observa-tions (Arzoumanian et al. 2018); these were taken between MJDs 56139 and 57015 (2012 July 31 to 2014 December 23), which were used to test the suitability of this pulsar for pulsar timing arrays (PTAs). The pulsar was eventually dropped out of the PTA. To this we added the ToAs from a dense, targeted
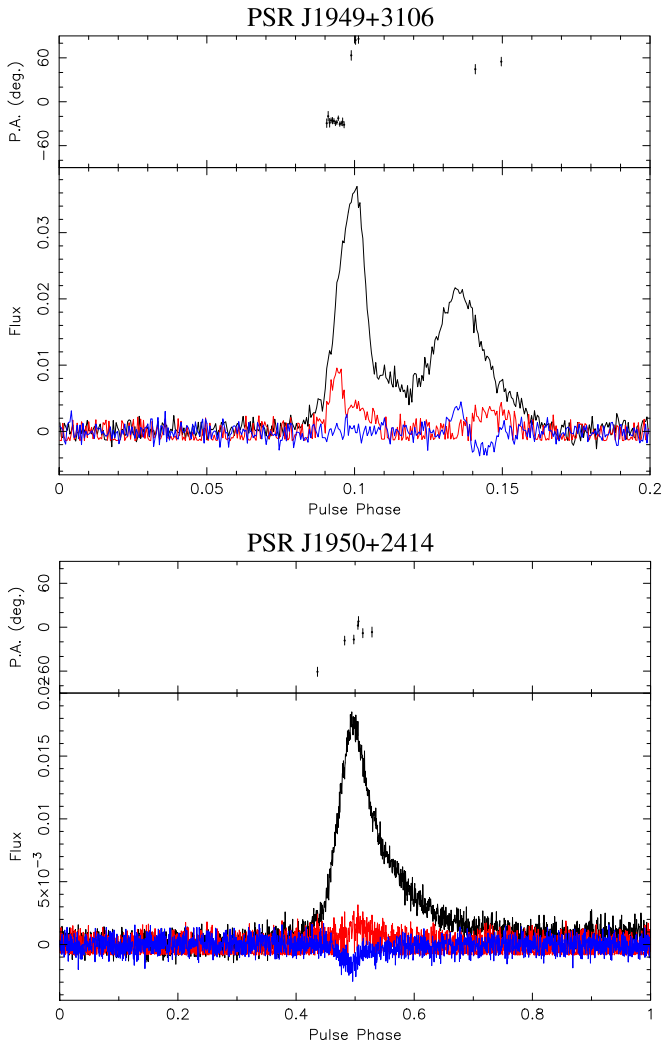
---

[20] http://psrchive.sourceforge.net/index.shtml

Figure 1. Polarization profiles for PSR J1949+3106 (top, zoomed in on spin phase between 0 and 0.2) and PSR J1950+2414 (bottom) obtained with the Arecibo *L*-band receiver (1150–1730 MHz). For the latter pulsar, the effects of scattering are evident. The black lines indicate the total intensity, the red lines the amount of linear polarization, and the blue lines the amount of circular polarization. The panels above each profile show the position angle (PA) of the linear polarization.

orbital campaign that happened between MJDs 57839 and 57887 (2017 March 27 and May 14).

For PSR J1950+2414, most of the additional data were obtained during two dense orbital campaigns, the first between MJDs 56557 and 56576 (2013 September 22 to October 11) and the second between MJDs 57725 and 57744 (2016 December 3 to 22), with more sparse observations made at other times.

The ToA analysis is made using `tempo`.[21] To convert the telescope ToAs (corrected to the International Bureau of Weights and Measures version of Terrestrial Time, TT) to the solar system barycenter, we used the Jet Propulsion Laboratory's DE 436 solar system ephemeris; the resulting timing parameters are presented in Barycentric Dynamical Time (TDB).

The timing solutions for both pulsars are presented in Table 1. All uncertainties are as derived by TEMPO, and quoted to 1σ (68.3% C. L.). For each pulsar, we present two solutions,

---

[21] http://tempo.sourceforge.net/ (Nice et al. 2015).

one based on the DDGR orbital model (Damour & Deruelle 1986), which assumes the validity of GR to derive self-consistent mass values, and a second solution based on a theory-independent parameterization of the relativistic effects observed in the timing of these systems, the DD model (Damour & Deruelle 1986) with a reparameterization of the Shapiro delay known as the "orthometric" parameterization (Freire & Wex 2010). Its implementation in `tempo` has the name DDFWHE (Weisberg & Huang 2016). The ToA residuals obtained with the DDGR solutions for PSRs J1949+3106 and J1950+2414 are presented in Figures 2 and 3, respectively.

We modeled the DM by introducing DM derivatives, seven in the case of PSR J1949+3106 and six in the case of J1950+2414. The number of derivatives was determined by the significance of the improvement; we stopped adding new derivatives when the χ^2 improvement became smaller than 2.

For PSR J1949+3106, we investigated the possibility of using the DMX model, which fits for a time-varying DM (Demorest et al. 2013). In this model we selected ranges of 6 days for independent DM estimates, as in the NANOGrav data analysis (Arzoumanian et al. 2018); the measured DM values are presented in the top plot of Figure 2, as a function of time. We only present the DM offsets of time segments with TOAs measured at multiple frequencies; these were only derived for Arecibo data, where we obtained independent TOAs for every 100 MHz subband of the *L*-wide data. The problem of this approach is that the mass values are strongly dependent on the DMX interval we choose to use. This stems, we believe, from the fact that we only have data taken at the *L* band. Multi-receiver data would be necessary to make more robust measurements of the DM variations in a way that the uncertainties do not affect the small time signatures from the Shapiro delay.

3. Results

3.1. Proper Motions

For both systems we can measure precise proper motions, with total magnitude μ and a position angle Θ_μ given in Table 1, both in Equatorial (J2000) and Galactic coordinates. For both pulsars, this has some covariance with the DM variations; for this reason the proper motion and velocity uncertainties are underestimated.

Both systems have Westwards proper motions along the Galactic plane. The vertical velocities (i.e., the heliocentric velocities in the direction perpendicular to the Galactic plane) are small: $v_V = \mu \cos(\Theta_\mu) d_{\text{psr}} = (-0.63 \pm 0.16) \times d_{\text{J1949+3106}}$ km s^{-1} and $v_V = (-0.3 \pm 0.9) \times d_{\text{J1950+2414}}$ km s^{-1}, where d_{psr} are their distances. We cannot measure the parallaxes from the timing with any significance, so we derive the distances from their DMs using the NE2001 (Cordes & Lazio 2002) and the YMW16 (Yao et al. 2017) models of the Galactic electron distribution; these are presented in Table 1. Assuming the YMW16 distances for both systems, their vertical velocities are -4.8 ± 1.2 and -2.3 ± 6.6 km s^{-1}, respectively. The vertical velocity of the Sun in the Galaxy is about $+7.3(1.0)$ km s^{-1} (Schönrich et al. 2010); this means that all objects with no vertical velocity are seen, in the heliocentric frame, with an opposite vertical velocity. Subtracting that from the observed proper motions, we obtain, in the reference frame of the Galaxy, $v_V = 2.5 \pm 1.2$ and 5.0 ± 6.6 km s^{-1}, respectively.

Table 1
Ephemerides for Two Binary Pulsars

PSR	J1949+3106		J1950+2414	
Observation and Data Reduction Parameters				
Reference epoch (MJD)	56000		56000	
Span of timing data (MJD)	54389–57887		55838–57883	
Number of ToAs	3441		913	
Assumed Solar wind parameter, n_0 (cm^{-3})	0		6	
rms Residual (μs)	3.8	3.8	4.7	4.7
χ^2	3629.6	3629.7	908.4	908.6
Reduced χ^2	1.063	1.063	1.023	1.023
Astrometric and Spin Parameters				
R.A., α (J2000)	19:49:29.6374604(37)	19:49:29.6374604(37)	19:50:45.063662(24)	19:50:45.063661(24)
Decl., δ (J2000)	31:06:03.80604(7)	+31:06:03.80604(6)	+24:14:56.9639(4)	+24:14:56.9639(4)
Proper motion in α, μ_α (mas yr^{-1})	−2.895(31)	−2.894(31)	−2.12(18)	−2.12(18)
Proper motion in δ, μ_δ (mas yr^{-1})	−5.091(46)	−5.093(45)	−3.63(19)	−3.64(19)
Spin frequency, ν (Hz)	76.1140249316118(7)	76.1140249316119(6)	232.300152212241(37)	232.300152212240(37)
Spin frequency derivative, $\dot{\nu}$ (10^{-15} Hz s^{-1})	−0.544131(7)	−0.544131(7)	−1.01478(37)	−1.01477(37)
Dispersion measure, DM (cm^{-3} pc)	164.1266824	164.12669(24)	142.0842(31)	142.0842(31)
Rotation measure, RM (cm^{-3} pc)	230(20)	230(20)	⋯	⋯
Binary Parameters				
Orbital model	DDFWHE	DDGR	DDFWHE	DDGR
Orbital period, $P_{\rm b}$ (days)	1.9495374(6)	1.94953755(20)	22.19137127(6)	22.19137127(6)
Projected semimajor axis, x (lt-s)	7.2886512(13)	7.2886510(7)	14.2199356(8)	14.21993591(35)
Epoch of periastron, T_0 (MJD)	56000.58744(47)	56000.58740(44)	56001.3656142(26)	56001.3656143(26)
Orbital eccentricity, e	0.000043124(36)	0.000043122(35)	0.07981175(6)	0.07981173(4)
Longitude of periastron, ω (°)	207.87(9)	207.86(8)	274.47042(4)	274.47042(5)
Total mass, M ($M_\odot$)	1.99[a]	2.124(20)	1.7790[a]	1.779(25)
Companion mass, M_c ($M_\odot$)	0.81[b]	0.81(5)	0.300[b]	0.2788(38)
Rate of advance of periastron, $\dot{\omega}$ (° yr^{-1})	0.103(19)	⋯	0.001678(16)	⋯
Orthometric amplitude of Shapiro delay, h_3 (μs)	2.33(7)	⋯	0.71(12)	⋯
Orthometric ratio of Shapiro delay, ς	0.837(12)	⋯	0.783346[c]	⋯
Derivative of $P_{\rm b}$, $\dot{P}_{\rm b}$ (10^{12} s s^{-1})	−0.046(28)	−0.037(25)[d]	−1(11)	0(11)[d]
Derived Parameters				
Galactic longitude, l	66.8583	66.8583	61.0975	61.0975
Galactic latitude, b	2.5536	2.5536	−1.1687	−1.1687
DM-derived distance, $d_{\rm psr,1}$ (kpc)	6.5	6.5	5.6	5.6
DM-derived distance, $d_{\rm psr,2}$ (kpc)	7.5	7.5	7.3	7.3
Galactic height, $Z_{\rm psr,1}$ (kpc)	0.29	0.29	0.11	0.11
Galactic height, $Z_{\rm psr,2}$ (kpc)	0.33	0.33	0.15	0.15
Magnitude of proper motion, μ (mas yr^{-1})	5.856(43)	5.858(42)	4.21(19)	4.21(19)
Heliocentric transverse velocity, $v_{\rm T}$ (km s^{-1})	208(31)	208(31)	145(22)	145(22)
Position angle of proper motion, Θ_μ (deg, J2000)	209.62(34)	209.60(34)	210.2(2.5)	210.2(2.5)
Θ_μ (deg, Galactic)	268.69(34)	268.67(34)	269.2(2.5)	269.1(2.5)
Pulsar spin period, P (ms)	13.13818315216540(12)	13.13818315216539(11)	4.3047754832565(7)	4.3047754832565(7)
Spin period derivative, $\dot{P}$ (10^{-20} s s^{-1})	9.39235(13)	9.39235(13)	1.8805(7)	1.8805(7)
Intrinsic spin period derivative, $\dot{P}_{\rm int}$ (10^{-20} s s^{-1})	$9.40^{+0.48}_{-0.78}$	$9.40^{+0.48}_{-0.78}$	$2.033^{+0.003}_{-0.014}$	$2.033^{+0.003}_{-0.014}$
Surface magnetic flux density, B_0 (10^9 Gauss)	1.12	1.12	0.30	0.30
Characteristic age, τ_c (Gyr)	2.2	2.2	3.4	3.4
Spin-down power, $\dot{E}$ (10^{33} erg s^{-1})	1.6	1.6	10.1	10.1
Mass function, f ($M_\odot$)	0.10938583(8)	0.10938582(5)	0.0062691312(11)	0.0062691316(5)
Pulsar mass, M_p ($M_\odot$)	⋯	1.33(15)	⋯	1.500(22)
Orbital inclination (deg)	79.9	79.9	76.1	76.1

Notes. Timing parameters derived using TEMPO, derived in the Barycentric Dynamical Time (TDB), using DE 436 solar system ephemeris. d_1 is derived using the NE2001 (Cordes & Lazio 2002) Galactic model, d_2 using the YMW16 (Yao et al. 2017) Galactic model. Estimate of $v_{\rm T}$, $\dot{P}_{\rm int}$ assumes d_2 with an uncertainty of 15%.
[a] Derived from $\dot{\omega}$.
[b] Derived from h_3 and ς.
[c] Assumed from best inclination given by the DDGR fit.
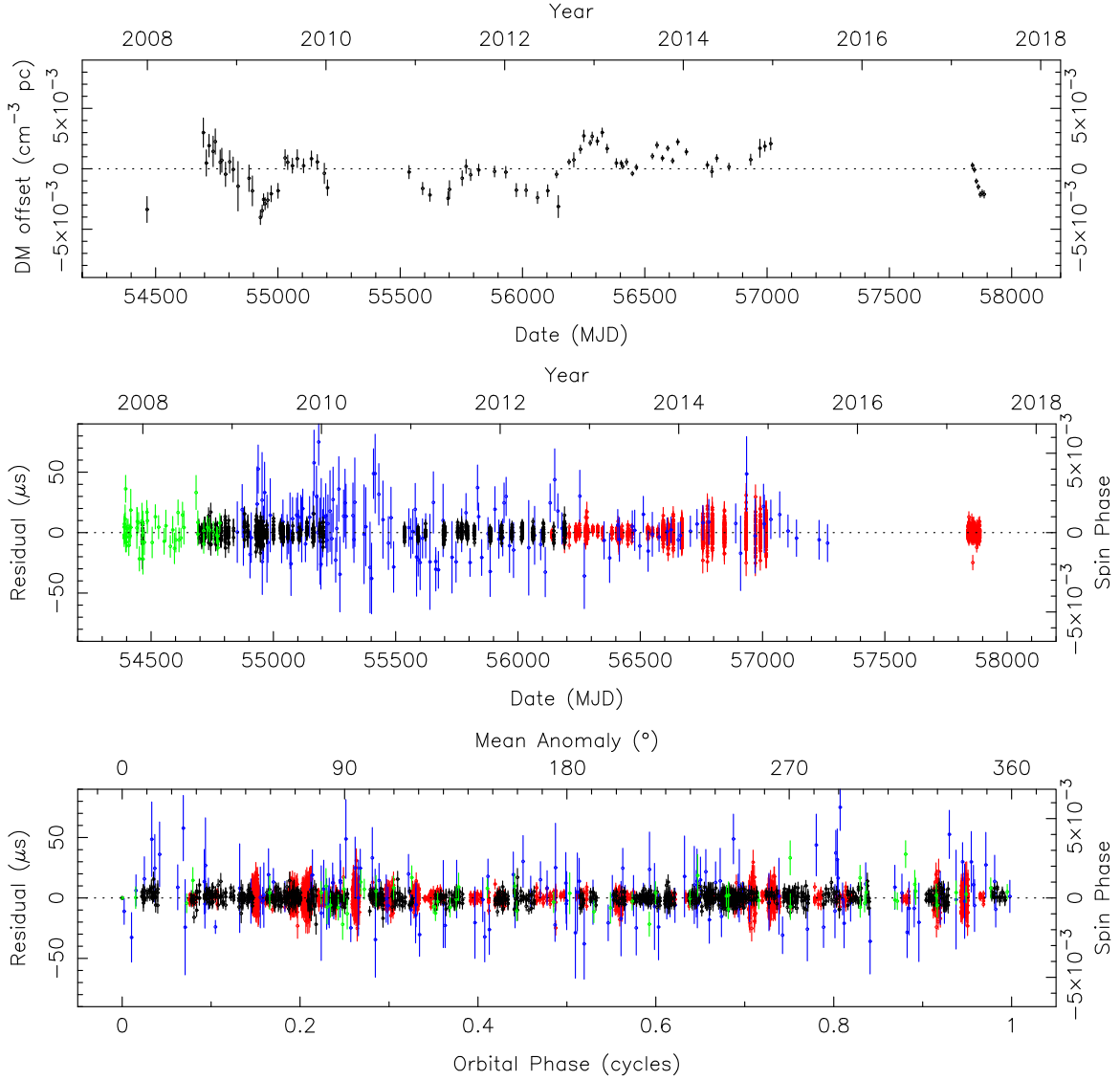[d] Fitted as the XPBDOT parameter.

Figure 2. Top: dispersion measure offsets of PSR J1949+3106 relative to the DM fixed in Table 1 as a function of date; these are obtained using a DMX-type ephemeris. We only present the DM offsets of time segments with TOAs measured at multiple frequencies; these were only derived for Arecibo data. Post-fit ToA residuals for all TOA data sets using the DDGR ephemeris in Table 1 (which used DM derivatives, not the DMX parameterization) as a function of (middle) date and (bottom) orbital phase. The residual 1σ uncertainties are indicated by vertical error bars. Black indicates data taken with the WAPP correlators, red indicates data taken with PUPPI, blue indicates data taken at Jodrell Bank with the ROACH system, and green indicates data taken with the GBT.

The vertical velocities are a component of the pulsar's velocity relative to the local standard of rest (LSR), known as peculiar velocity. The fact that they are small suggests that the pulsars might be in the LSR. We now test this hypothesis by calculating the magnitude of the proper motions parallel the Galactic plane (the horizontal proper motions) these pulsars should have if they were in the LSR.

The first step is to calculate the X, Y, and Z coordinates of the pulsar, which is done easily enough from l, b, and d and the Sun's distance to the Galactic center, r_0. For this, we used the estimate from the GRAVITY experiment (Gravity Collaboration et al. 2018), $r_0 = 8.122(31)$ kpc. The coordinates for the Sun are $X_\odot = r_0$, $Y_\odot = 0$, and $Z_\odot \simeq 0.02$; for the pulsar $X_{\rm psr} = r_0 - d_{\rm psr}\cos(l)\cos(b)$, $Y_{\rm psr} = d_{\rm psr}\sin(l)\cos(b)$, and $Z_{\rm psr} = Z_\odot + d_{\rm psr}\sin(b)$.

The Sun's peculiar velocity is given by $V_{X,\odot} = -11.1(1.5)$, $V_{Y,\odot} = 12.2(2.0)$ and $V_{Z,\odot} = 7.3(1.0)\,{\rm km\,s^{-1}}$ (here the X direction is away from the center of the Galaxy, the opposite of the

convention used by Schönrich et al. 2010, which defines the X axis as pointing to the center of the Galaxy). To get the velocity of the Sun relative to the Galactic center, we add the Galaxy's rotational velocity to $V_{Y,\odot}$. Here we use the value provided by McGaugh (2018), $v_{\rm Gal} = 233.3\,{\rm km\,s^{-1}}$, which already takes the updated r_0 into account.

If the pulsar is in the LSR, then $V_{X,{\rm psr}} = -v_{\rm Gal}Y_{\rm psr}/r_{\rm psr}$ and $V_{Y,{\rm psr}} = v_{\rm Gal}X_{\rm psr}/r_{\rm psr}$, where $r_{\rm psr}$ is the pulsar's distance from the Galactic center. Finally, we calculate the projection of the difference of velocities along a unit vector perpendicular to the line of sight and parallel to the plane of the Galaxy, and then divide the resulting velocity by the distance to the pulsar to obtain the horizontal proper motion μ_H.

For PSR J1949+3106 ($l = 66^\circ.8583$) the NE2001 distance is 6.5 kpc, and $r_{\rm psr} = 8.18$ kpc, a distance very similar to r_0. From this we obtain $\mu_H = -5.85\,{\rm mas\,yr^{-1}}$, where the negative sign indicates Westwards motion along the Galactic plane (thus, decreasing l). For the YMW16 distance (7.5 kpc),
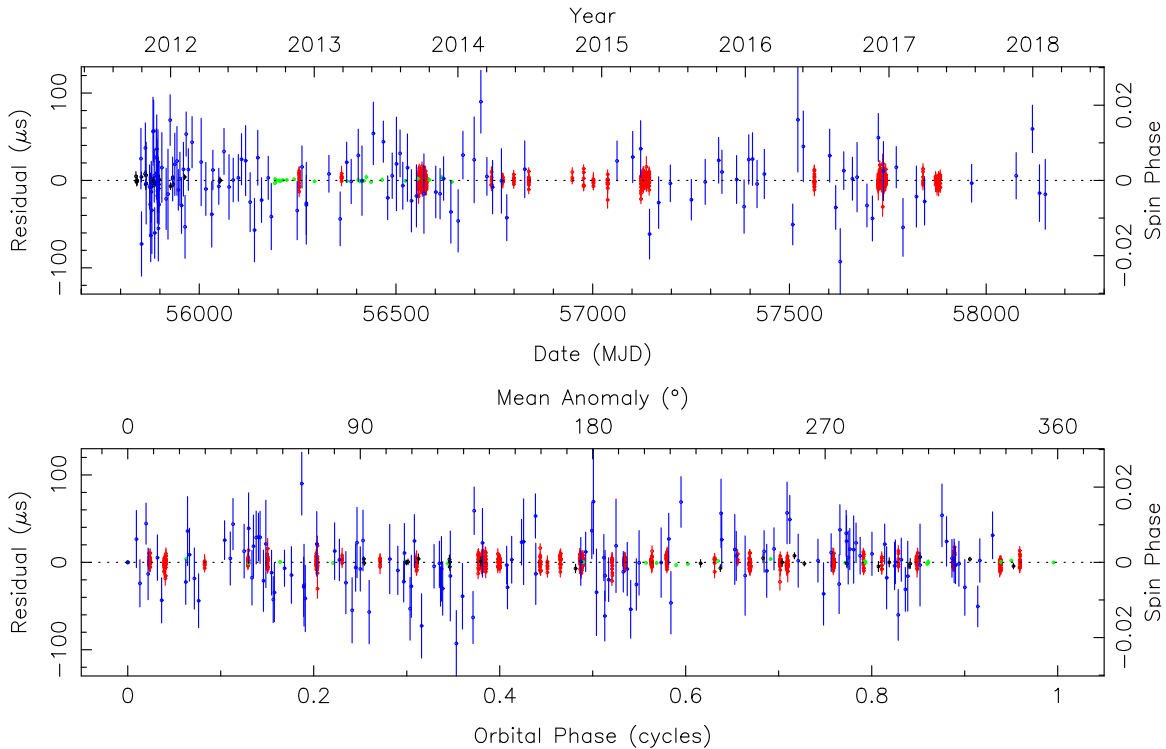
Figure 3. ToA residuals for the DDGR ephemeris of PSR J1950+2414 in Table 1 as a function of (top) date and (bottom) orbital phase. The residual 1σ uncertainties are indicated by vertical error bars. Black indicates data taken with the Mock spectrometers, green indicates data taken with PUPPI in incoherent mode, red indicates data taken with PUPPI in coherent mode, and blue indicates data taken at Jodrell Bank with the ROACH system.

$r_{\rm psr} = 8.60\,{\rm kpc}$ and $\mu_H = -5.69\,{\rm mas\,yr}^{-1}$. The observed μ_H, given by $\mu\sin(\Theta_\mu) = -5.86(4)\,{\rm mas\,yr}^{-1}$, is in very good agreement with the NE2001 estimate and in 4.3σ disagreement with the YMW16 estimate. If the NE2001 distance is correct, the peculiar horizontal velocity of the pulsar is $v_H = 0.0(1.3)\,{\rm km\,s}^{-1}$; if the YMW16 model distance is correct, $v_H = 5.9(1.5)\,{\rm km\,s}^{-1}$. Thus, the precision of v_H is limited by the uncertainty of the distance. If we assume that the pulsar is in the LSR, then the NE2001 distance estimate is much closer to the real distance than the YMW16 estimate.

For PSR J1950+2414 ($l = 61°.0975$) the NE2001 distance is 5.6 kpc, thus $\mu_H = -6.11\,{\rm mas\,yr}^{-1}$. For the YMW16 distance (7.3 kpc) $\mu_H = -6.04\,{\rm mas\,yr}^{-1}$. The observed horizontal proper motion, $\mu_H = -4.21(19)\,{\rm mas\,yr}^{-1}$, is in clear disagreement with the estimates above; the differences are $+1.90(19)$ and $+1.83(19)\,{\rm mas\,yr}^{-1}$. This is about 10σ significant in both cases. Using the YMW16 distance, we obtain $v_H = +61(7)\,{\rm km\,s}^{-1}$. Thus, PSR J1950+2414 has a significant horizontal peculiar velocity, despite its very small vertical velocity.

3.2. DM Evolution

If PSR J1949+3106 were in the LSR, and if $r_{\rm psr} \simeq r_0$ (this happens if the pulsar is near the NE2001 distance), then something interesting would happen: the pulsar and the Sun would not only travel with nearly the same absolute velocity as all objects in the LSR ($v_{\rm gal}$), but they would also have approximately the same angular velocity ($\Omega_{\rm gal} = v_{\rm gal}/r_0$) around the Galactic center. In such a configuration, the Sun and PSR J1949+3106 would form an approximately rigid rotating triangle, i.e., one with approximately constant side length. Thus, the distance between the Sun and PSR J1949+3106 would change little, i.e., J1949+3106 should have a very small

heliocentric radial velocity. A detailed calculation yields a radial velocity of $-16.9\,{\rm km\,s}^{-1}$ that is mostly caused by the Sun's peculiar velocity; without the latter, the radial velocity would be $-1.3\,{\rm km\,s}^{-1}$.

Currently, it is not possible to measure the heliocentric radial velocity of this system: the quantity cannot be extracted from pulsar timing. It could in principle be extracted from absorption lines in the optical spectrum of the companion; however, the companion to PSR J1949+3106 has not been detected. For this reason, we cannot measure the peculiar velocity of PSR J1949+3106 along the radial direction, so we cannot conclude that the system really has a low peculiar velocity, even though this is true in the direction perpendicular to the line of sight.

Recently, Jones et al. (2017) used the observed DM variations of the NANOGrav MSPs in an attempt to measure the radial velocities of the pulsars. A detailed calculation of all effects is beyond the scope of this work. However, if the pulsar and the intervening ionized interstellar medium (IISM) are all in the LSR, then there should be very little change in the line of sight of the system relative to the IISM, since the latter is basically comoving with the Earth and the system. This means that there should be no long-term increasing or decreasing trend in the DM of the pulsar. This is in agreement with the observations presented in Figure 2—the DM derivative is $0.00060(20)\,{\rm cm}^{-3}\,{\rm pc\,yr}^{-1}$, 3σ consistent with zero—and in disagreement with the DM trends observed for most other pulsars listed by Jones et al. (2017).

3.3. Spin Parameters

With the assumed distances and the measured proper motion we can estimate the magnitude of the kinematic effects that may bias the timing parameters using the simple expressions

provided by Shklovskii ([1970](#)) and Damour & Taylor ([1991](#)), which estimate the rate of change of the Doppler shift factor D:

$$\frac{\dot{D}}{D} = -\frac{a_l + \mu^2 d}{c}. \tag{1}$$

To estimate the Galactic acceleration a_l, we use the equations provided by Lazaridis et al. ([2009](#)). These are reasonably accurate for these pulsars since they are very close to the Galactic plane. In those equations we used the r_0 and v_{Gal} from the previous section. The results for $\dot{D}/D$ are $0.5^{+3.6}_{-5.9} \times 10^{-20}$ s^{-1} and $35.6^{+0.6}_{-3.3} \times 10^{-20}$ s^{-1} for J1949+3106 and J1950+2414, respectively, both values calculated assuming the YMW16 distances. The expected value for PSR J1949+3106 (consistent with zero) is consistent with the "rigid rotating triangle" configuration mentioned above where the distance between the pulsar and the Earth is unchanging: indeed, $\dot{D}$ is proportional to the second derivative of that distance.

With the values of $\dot{D}/D$ for both pulsars, we can estimate the kinematic correction to the spin period derivatives, $\dot{P}_{kin} = -P\dot{D}/D$. Subtracting this from the observed $\dot{P}$s we obtain intrinsic spin period derivatives ($\dot{P}_{int}$); these are quite similar to the observed values for both pulsars. From P and $\dot{P}_{int}$, we derive updated values for the characteristic age (τ_c), surface magnetic flux density (B_0), and also the rate of loss of rotational energy ($\dot{E}$) using the standard expressions presented by Lorimer & Kramer ([2004](#)). All these quantities are presented in Table [1](#).

3.4. Orbital Period Derivatives

The observed orbital period derivative for these binaries with compact companions is given, to first order, by

$$\left(\frac{\dot{P}_b}{P_b}\right)_{obs} = \left(\frac{\dot{P}_b}{P_b}\right)_{GW} - \frac{\dot{D}}{D}, \tag{2}$$

where the first term is the orbital decay caused by the emission of gravitational waves and the second term is the fractional rate of change of the Doppler shift calculated in Equation ([1](#)).

In the case of PSR J1950+2414, it is clear that only the second term matters. Indeed, in that case the DDGR model predicts $\dot{P}_{b,GR} = -4.47 \times 10^{-17}$ s s^{-1}; this is four orders of magnitude smaller than the kinematic term $\dot{P}_{b,k} \equiv -P_b\dot{D}/D = -0.68^{+0.06}_{-0.01} \times 10^{-12}$ s s^{-1}. If we fit for this quantity, we obtain $\dot{P}_{b,obs} = -1 \pm 11 \times 10^{-12}$ s s^{-1}. This means we are one order of magnitude away from the detection of $\dot{P}_{b,k}$.

For PSR J1949+3106, the situation is far more interesting. In that case, $\dot{P}_{b,GR} \simeq -6 \times 10^{-15}$ s s^{-1} is comparable to the uncertainty of the kinematic term $\dot{P}_{b,k} = -0.8^{+10.0}_{-6.1} \times 10^{-15}$ s s^{-1}, obtained assuming the YMW16 distance with a 15% uncertainty. Our DDFWHE solution yields $\dot{P}_{b,obs} = -46 \pm 56 \times 10^{-15}$ s s^{-1} (95.4% C. L.). This precision is not yet enough to constrain the distance to the system.

3.5. Mass Measurements

For each pulsar in this work, we detect three post-Keplerian parameters: the rate of advance of periastron ($\dot{\omega}$), and the Shapiro delay, which yields two parameters, the orthometric amplitude (h_3) and ratio (ς). The fits made using the DDGR model (Damour & Deruelle [1986](#)) use the relativistic time signatures of these effects and assume the validity of GR to

provide direct estimates of the total binary mass M and the companion mass M_c. For PSR J1949+3106, these are respectively $M = 2.14(20)\,M_\odot$, $M_c = 0.81(5)\,M_\odot$, and $M_p = 1.33(15)\,M_\odot$; given the mass function these correspond to $s = \sin i \simeq 0.9844$ .... These are 1σ consistent with the values presented by Deneva et al. ([2012](#)), but are ~ 2 times more precise. These masses are based almost entirely on the measurement of the Shapiro delay (see Figure [4](#)), but are now being influenced by the detection of $\dot{\omega}$.

One of the remarkable features of PSR J1949+3106 is that we have a 5σ significant measurement of $\dot{\omega}$ of this system despite the fact that its orbital eccentricity is rather small ($e = 4.3124(36) \times 10^{-5}$). The value we measure, $\dot{\omega} = 0°.103(19)$ yr^{-1}, is consistent with the the GR prediction for the masses determined from the Shapiro delay (see Figure [4](#)). This is a test of GR, although not a very constraining one.

For PSR J1950+2414, the DDGR solution yields precise masses: the total mass is $M = 1.779(25)\,M_\odot$; for the individual masses we obtain $M_c = 0.2788(38)\,M_\odot$ and $M_p = 1.500(22)\,M_\odot$.

The total mass is determined precisely because the unusually large eccentricity of the system ($e = 0.07981175(6)$) enables a precise measurement of the rate of advance of periastron ($\dot{\omega} = 0°.001678(16)$ yr^{-1} in the DDFWHE solution). The constraints imposed by this, assuming that the effect is caused by GR alone, are shown with the red lines in Figure [5](#).

The Shapiro delay yields, on its own, far less precise masses than for PSR J1949+3106; fitting for both h_3 and ς we get very low significance for both parameters. To better estimate the regions allowed by the Shapiro delay, we fix ς to the value of $\sin i$ derived by the DDGR solution ($s = \sin i = 0.9709 ...$), using (Freire & Wex [2010](#))

$$\varsigma = \frac{s}{1 + \sqrt{1 - s^2}} = 0.7833... \tag{3}$$

this is represented by the blue dashed lines in Figure [5](#). With this, we obtain a highly significant detection of the orthometric amplitude, $h_3 = 0.71 \pm 0.12\,\mu s$. It is this constraint, in combination with the $\dot{\omega}$, that allows the precise measurement of the individual component masses (see Figure [5](#)).

We now verify whether the $\dot{\omega}$ is caused by the effects of GR. To do this, we estimate the contribution to $\dot{\omega}$ from the proper motion of the system ($\mu = 4.21(19)$ mas yr^{-1}), using the equations first derived by Kopeikin ([1995](#), [1996](#)). The largest possible contribution is given by

$$\dot{\omega}_k = \pm\frac{\mu}{\sin i} = \pm 1.2 \times 10^{-6}\,\text{deg yr}^{-1}, \tag{4}$$

which is one order of magnitude smaller than the uncertainty of $\dot{\omega}$. Other contributions are likely to be smaller (Stovall et al. [2019](#)). Therefore, the assumption that the measured $\dot{\omega}$ is relativistic is, to our knowledge, warranted.

3.6. Bayesian Mass Estimates

To verify the uncertainty estimates for the masses, we used the Bayesian method described in detail by Barr et al. ([2017](#)) and references therein. In this method, we make a map of the χ^2 of the ToA residuals as a function of $\cos i$ (which has a constant probability for randomly oriented orbits) and h_3 in the case of PSR J1949+3106 (in order to save computational time from being allocated to regions with very bad values of χ^2), and M_c in the case of PSR J1950+2414. We then transform these χ^2 maps
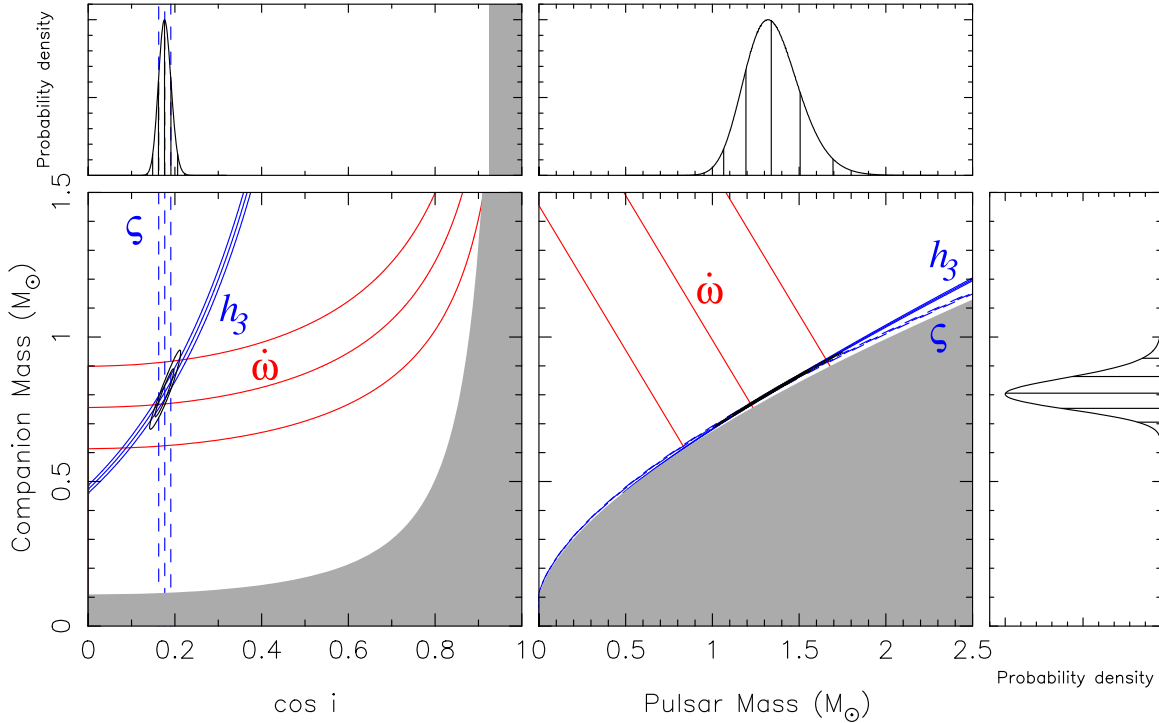
Figure 4. Mass constraints for PSR J1949+3106. In the main square plots, the lines indicate the regions that are (according to general relativity) consistent with the nominal and $\pm 1\sigma$ measurements of h_3 (solid blue), ς (dashed blue), and $\dot{\omega}$ (solid red) obtained from the DDFWHE model (see Table 1). The contour plots include 68.23% and 95.44% of the total two-dimensional probability density function (pdf), derived from the quality (χ^2) of the TEMPO fits using a DDGR model to the ToA data set we have obtained for this pulsar. The location of the regions of high probability is well described by the h_3 and ς parameters and their uncertainties, with a small influence from $\dot{\omega}$. In the left plot, we display the cosine of the orbital inclination (cos i, which has, for randomly inclined orbits, a flat pdf) vs. the companion mass (M_c); the gray region is excluded because the pulsar mass (M_p) must be larger than 0. In the right plot, we display M_p vs. M_c; the gray region is excluded by the constraint sin $i \leqslant 1$. The side panels display the 1D pdfs for cos i (top left), M_p (top right), and M_c (right). The vertical lines in these pdfs indicate the median and the percentiles corresponding to 1σ and 2σ around the median.

into a 2D probability density function (pdf) in the cos i–M_c plane; we also translate it into a similar pdf in the M_p–M_c plane. The contours holding 68.23% and 95.44% of all probability in these planes are displayed in Figures 4 for PSR J1949+3106 and 5 for PSR J1950+2414. For the former, the region of high probability is well described by the orthometric Shapiro-delay parameters, h_3 and ς, and their uncertainties, as predicted by Freire & Wex (2010) and already observed in this system by Deneva et al. (2012). For the latter system, the region of high probability is well described by h_3, $\dot{\omega}$, and their uncertainties. Projecting these 2D pdfs onto the different axes, we obtain the probabilities for the masses and orbital inclination. For PSR J1949+3106 the 68.3% confidence limits are $M_c = 0.81^{+0.06}_{-0.05}\,M_\odot$, $M_p = 1.34^{+0.17}_{-0.15}\,M_\odot$, and $i = 79.9^{+0.8}_{-0.9}$ deg; for PSR J1950+2414 $M_c = 0.2795^{+0.0046}_{-0.0038}\,M_\odot$, $M_p = 1.496 \pm 0.023\,M_\odot$, and $i = 75.7^{+2.2}_{-2.8}$ deg. For both systems, these values and uncertainties are in good agreement with those obtained using the DDGR model in TEMPO.

4. Discussion

4.1. PSR J1949+3106

The companion WD to this pulsar has a mass of about 0.8 $M_\odot$; this suggests it is a carbon–oxygen WD. The pulsar in this system seems to have a rather normal mass ($M_p = 1.34\,M_\odot$); although, in this case the precision of the measurement is still consistent, within 2σ, with a wide range of masses, from 1.06 to 1.70 $M_\odot$. This means that improvements on the mass measurements are still of scientific interest. Since the

measurement precision for $\dot{\omega}$ improves faster than for the Shapiro-delay parameters (the uncertainties decrease as $T^{-3/2}$ for the former versus $T^{-1/2}$ for the latter, where T is the timing baseline), it is likely that, in a not-too-distant future, the combination of $\dot{\omega}$ with the Shapiro-delay parameters will yield much more precise masses, as in the case of the other pulsar described in this work, PSR J1950+2414. If we set the uncertainty of M to zero in the DDGR model, we can simulate the results we would obtain for this system if we measured a very precise $\dot{\omega}$. In that case, the individual masses can be measured with an uncertainty of only $\sim 7.5 \times 10^{-4}\,M_\odot$ from the combination of the "fixed" $\dot{\omega}$ and h_3.

The characteristics of this system suggest a relatively mild evolutionary history. The small transverse peculiar velocity indicates that the kick associated with the supernova that formed this neutron star was unusually small, even though its effect on the peculiar motion of the system would have been attenuated by the large mass of the progenitor of the WD companion. This suggests that the envelope of the progenitor to PSR J1949+3106 was heavily stripped by the progenitor of the companion WD.

In double neutron star systems, there seems to be a positive correlation between the kick magnitude and the mass of the second-formed NS (Tauris et al. 2017). If kick magnitude is also correlated with the mass for the first-formed NS in NS–WD systems, then the small velocity of PSR J1949+3106 relative to the LSR and the small implied kick would suggest a relatively small mass for PSR J1949+3106.
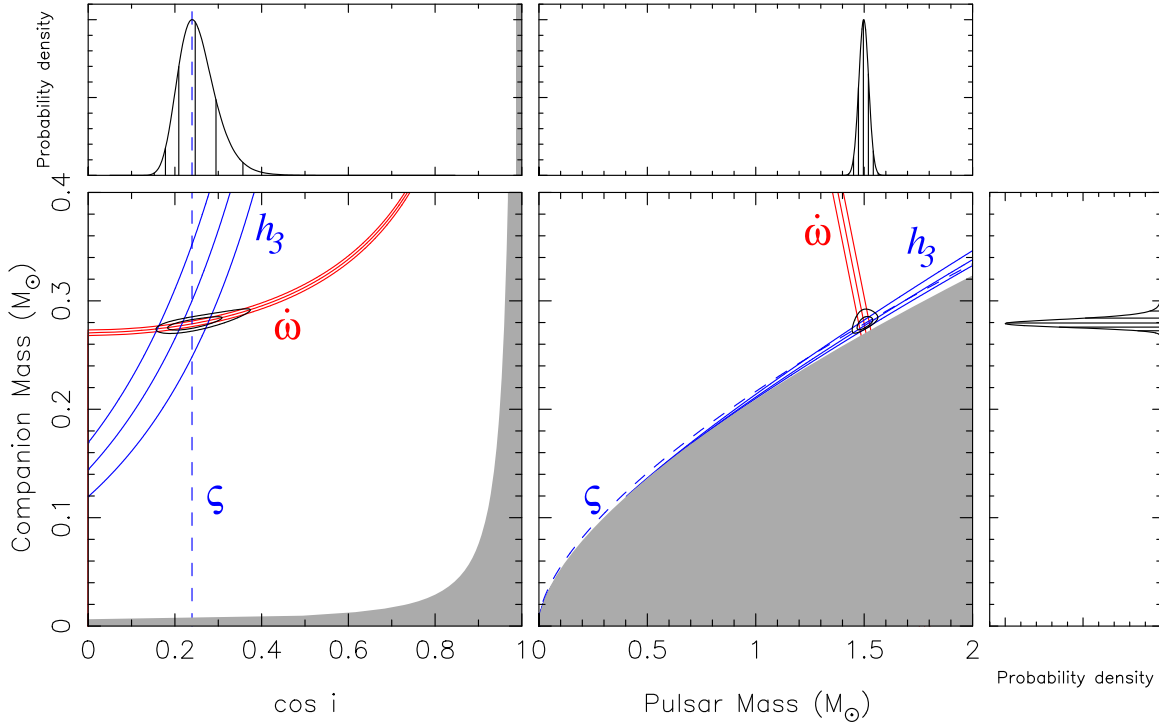
Figure 5. Same as Figure 4, but this time for PSR J1950+2414. One of the differences is the much larger uncertainties for h_3 and ς described in the text; for that reason we fixed ς to the value predicted by the best DDGR ephemeris in Table 1, and then fitted for h_3 independently. As in Figure 4, the probability density functions are obtained with a fully self-consistent DDGR model. The regions of higher probability are reasonably well described by the $\dot{\omega}$ and h_3 parameters and their uncertainties.

4.2. PSR J1950+2414

As discussed already by Knispel et al. (2015) and in Section 1, the second object studied in this work, PSR J1950 +2414, is a member of a recent and growing class of MSPs with unexplained large ($e \sim 0.1$) orbital eccentricities and orbital periods between 22 and 32 days.

Any measurements of the masses and proper motions for these intriguing systems, such as those we have obtained above, are important for testing the hypotheses that have been advanced for their formation. Apart from PSR J1950+2414, measurements have just been published for PSR J1946+3417 (Barr et al. 2017) and for PSR J2234+0611 (Stovall et al. 2019). As discussed in detail in these papers, these mass measurements exclude the hypotheses proposed by Freire & Tauris (2014) and Jiang et al. (2015), which are based on sudden mass loss of the MSP progenitor. All measurements thus far are consistent with the expectations of the hypothesis proposed by Antoniadis (2014). This proposes that the orbital eccentricity is caused by material ejected from the companion WD by nuclear reactions happening near its surface. This hypothesis predicts, among other things, that the MSPs in these systems should have a range of masses similar to those of the general MSP population (Antoniadis et al. 2016b; Özel & Freire 2016), which appears to be true.

Regarding the companions to the MSPs in these systems, the prediction of all hypotheses advanced to date is that they should be helium WDs with masses given by the Tauris & Savonije (1999) relation. The companion masses measured for PSR J1950+2414 (this work) and PSR J2234+0611 (Stovall et al. 2019) are in agreement with the Tauris & Savonije (1999) relation. Furthermore, optical observations of the companion of PSR J2234+0611 have confirmed that it is a He WD

(Antoniadis et al. 2016a). However, the companion mass measured for PSR J1946+3417 ($M_c = 0.2556(19)\ M_\odot$; Barr et al. 2017) is slightly smaller than that expectation.

One aspect that has not been discussed in detail until now has been the position of the eccentric MSPs in the P–$\dot{P}$ diagram. If, as predicted by Antoniadis (2014), these systems formed essentially as all other MSP binaries, they should be located in the same areas of the P–$\dot{P}$ diagram. This also appears to be the case as well.

ORCID iDs

W. W. Zhu https://orcid.org/0000-0001-5105-4058
P. C. C. Freire https://orcid.org/0000-0003-1307-9435
B. Allen https://orcid.org/0000-0003-4285-6256
S. Chatterjee https://orcid.org/0000-0002-2878-1502
J. M. Cordes https://orcid.org/0000-0002-4049-1882
F. Crawford https://orcid.org/0000-0002-2578-0360
J. S. Deneva https://orcid.org/0000-0003-1226-0793
R. D. Ferdman https://orcid.org/0000-0002-2223-1235
J. W. T. Hessels https://orcid.org/0000-0003-2317-1446
V. M. Kaspi https://orcid.org/0000-0001-9345-0307
R. Lynch https://orcid.org/0000-0001-5229-7430
S. M. Ransom https://orcid.org/0000-0001-5799-9714
K. Stovall https://orcid.org/0000-0002-7261-594X

References

Allen, B., Knispel, B., Cordes, J. M., et al. 2013, ApJ, 773, 91
Antoniadis, J. 2014, ApJL, 797, L24
Antoniadis, J., Freire, P. C. C., Wex, N., et al. 2013, Sci, 340, 448
Antoniadis, J., Kaplan, D. L., Stovall, K., et al. 2016a, ApJ, 830, 36
Antoniadis, J., Tauris, T. M., Ozel, F., et al. 2016b, arXiv:1605.01665
Archibald, A. M., Gusinskaia, N. V., Hessels, J. W. T., et al. 2018, Natur, 559, 73
Arzoumanian, Z., Brazier, A., Burke-Spolaor, S., et al. 2018, ApJS, 235, 37
Barr, E. D., Champion, D. J., Kramer, M., et al. 2013, MNRAS, 435, 2234
Barr, E. D., Freire, P. C. C., Kramer, M., et al. 2017, MNRAS, 465, 1711
Camilo, F., Kerr, M., Ray, P. S., et al. 2015, ApJ, 810, 85
Champion, D. J., Ransom, S. M., Lazarus, P., et al. 2008, Sci, 320, 1309
Cognard, I., Freire, P. C. C., Guillemot, L., et al. 2017, ApJ, 844, 128
Cordes, J. M., Freire, P. C. C., Lorimer, D. R., et al. 2006, ApJ, 637, 446
Cordes, J. M., & Lazio, T. J. W. 2002, arXiv:astro-ph/0207156
Crawford, F., Stovall, K., Lyne, A. G., et al. 2012, ApJ, 757, 90
Damour, T., & Deruelle, N. 1986, AIHPA, 44, 263
Damour, T., & Taylor, J. H. 1991, ApJ, 366, 501
Demorest, P. B., Ferdman, R. D., Gonzalez, M. E., et al. 2013, ApJ, 762, 94
Deneva, J. S., Freire, P. C. C., Cordes, J. M., et al. 2012, ApJ, 757, 89
Deneva, J. S., Stovall, K., McLaughlin, M. A., et al. 2013, ApJ, 775, 51
Donner, J. Y., Verbiest, J. P. W., Tiburzi, C., et al. 2019, A&A, 624, A22
Dowd, A., Sisk, W., & Hagen, J. 2000, in ASP Conf. Ser. 202, IAU Coll. 177, Pulsar Astronomy—2000 and Beyond, ed. M. Kramer, N. Wex, & R. Wielebinski (San Francisco, CA: ASP), 275
Freire, P. C. C., Bassa, C. G., Wex, N., et al. 2011, MNRAS, 412, 2763
Freire, P. C. C., & Tauris, T. M. 2014, MNRAS, 438, L86
Freire, P. C. C., & Wex, N. 2010, MNRAS, 409, 199
Freire, P. C. C., Wex, N., Esposito-Farèse, G., et al. 2012, MNRAS, 423, 3328
Gravity Collaboration, Abuter, R., Amorim, A., et al. 2018, A&A, 615, L15
Hotan, A. W., van Straten, W., & Manchester, R. N. 2004, PASA, 21, 302
Jiang, L., Li, X.-D., Dey, J., & Dey, M. 2015, ApJ, 807, 41
Jones, M. L., McLaughlin, M. A., Lam, M. T., et al. 2017, ApJ, 841, 125
Knispel, B., Allen, B., Cordes, J. M., et al. 2010, Sci, 329, 1305
Knispel, B., Lazarus, P., Allen, B., et al. 2011, ApJL, 732, L1
Knispel, B., Lyne, A. G., Stappers, B. W., et al. 2015, ApJ, 806, 140
Kopeikin, S. M. 1995, ApJL, 439, L5
Kopeikin, S. M. 1996, ApJL, 467, L93
Lazaridis, K., Wex, N., Jessner, A., et al. 2009, MNRAS, 400, 805
Lazarus, P., Brazier, A., Hessels, J. W. T., et al. 2015, ApJ, 812, 81
Lazarus, P., Freire, P. C. C., Allen, B., et al. 2016, ApJ, 831, 150
Lorimer, D. R., & Kramer, M. 2004, Handbook of Pulsar Astronomy (Cambridge: Cambridge Univ. Press)
Lorimer, D. R., Stairs, I. H., Freire, P. C., et al. 2006, ApJ, 640, 428
McGaugh, S. S. 2018, RNAAS, 2, 156
Nice, D., Demorest, P., Stairs, I., et al. 2015, Tempo: Pulsar Timing Data Analysis, Astrophysics Source Code Library, ascl:1509.002
Octau, F., Cognard, I., Guillemot, L., et al. 2018, A&A, 612, A78
Özel, F., & Freire, P. 2016, ARA&A, 54, 401
Ransom, S. 2011, PRESTO: PulsaR Exploration and Search TOolkit, Astrophysics Source Code Library, ascl:1107.017
Scholz, P., Kaspi, V. M., Lyne, A. G., et al. 2015, ApJ, 800, 123
Schönrich, R., Binney, J., & Dehnen, W. 2010, MNRAS, 403, 1829
Shklovskii, I. S. 1970, SvA, 13, 562
Spitler, L. G., Cordes, J. M., Hessels, J. W. T., et al. 2014, ApJ, 790, 101
Spitler, L. G., Scholz, P., Hessels, J. W. T., et al. 2016, Natur, 531, 202
Stovall, K., Allen, B., Bogdanov, S., et al. 2016, ApJ, 833, 192
Stovall, K., Freire, P. C. C., Antoniadis, J., et al. 2019, ApJ, 870, 74
Stovall, K., Freire, P. C. C., Chatterjee, S., et al. 2018, ApJL, 854, L22
Tauris, T. M., Kramer, M., Freire, P. C. C., et al. 2017, ApJ, 846, 170
Tauris, T. M., & Savonije, G. J. 1999, A&A, 350, 928
Thankful Cromartie, H., Fonseca, E., Ransom, S. M., et al. 2019, arXiv:1904.06759
Weisberg, J. M., & Huang, Y. 2016, ApJ, 829, 55
Yao, J. M., Manchester, R. N., & Wang, N. 2017, ApJ, 835, 29